

Adaptive control of structural intensity associated with bending waves in a beam

Allan E. Schwenk,^{a)} Scott D. Sommerfeldt, and Sabih I. Hayek

Department of Engineering Science and Mechanics and Applied Research Laboratory, The Pennsylvania State University, University Park, Pennsylvania 16802

(Received 9 June 1993; revised 7 March 1994; accepted 14 June 1994)

This paper examines a method to control adaptively the structural vibration intensity in a beam. An algorithm is developed to estimate the total, instantaneous structural intensity, using finite-difference techniques. In addition, algorithms based on the filtered- x least-mean-squares algorithm are developed to adaptively control the intensity. To investigate the effectiveness of adaptive control of structural intensity, a number of control actuator/error sensor configurations are used. Adaptive control is implemented at resonance and off-resonance frequencies, and the performance is evaluated by means of a separate accelerometer located in the structural far field. Experimental results demonstrate several trends. First, controlling the acceleration is considerably more effective when the error sensor is located in the far field rather than in the near field. Furthermore, controlling acceleration is more effective than controlling intensity, when the error sensors are in the far field. Conversely, when the error sensors are in the near field, the attenuation achieved by controlling intensity is comparable to or greater than that achieved by controlling acceleration.

PACS numbers: 43.40.Vn, 43.40.Cw

INTRODUCTION

Vibration control has long been a subject of interest in a large number of applications. Over the past few decades, there has been growing interest in the area of active vibration control for applications where passive control is ineffective. Nonadaptive active control of structural vibrations was studied in the 1950's, when Olson¹ generalized his "electronic sound absorber" to control vibrations. Adaptive control of structural vibrations was studied in the 1960's, when Bonesho and Bollinger² described how to build a "self-optimizing vibration damper." The device used an analog control circuit to vary the damper's stiffness. With recent developments in computer technology, most notably speed of processing, active control studies have become more prevalent. A large number of studies have been related to actively controlling flexible space structures. In this area, a number of control approaches and algorithms have been examined, including methods such as modal control and distributed-parameter control.³⁻⁶

In recent years, much research has also been performed applying and generalizing the filtered- x algorithm developed by Widrow and Stearns.⁷ Elliott *et al.* demonstrated how the filtered- x algorithm can be extended to control multiple error inputs.⁸ In 1990, Sommerfeldt and Tichy⁹ extended this approach to provide for real-time system identification and for multiple-error, multiple-output control. In 1991, Sommerfeldt¹⁰ applied this algorithm, most notably, to the case of four error sensors and four control actuators. A similar algorithm has also been developed to control sound fields.¹¹

There have been several studies of measurements of vibration intensity. In 1970, Noiseux¹² described a method for

measuring the "power flow" in beams. In 1984, Pavic¹³ described a method for measuring the intensity using an array of velocity transducers. His scheme employed a four-point finite-difference method to calculate the spatial derivatives needed to estimate the structural intensity. Recently, Hayek *et al.*¹⁴ studied several finite-difference methods that could be used to compute these spatial derivatives.

Fewer studies have investigated the control of vibration intensity. Redman-White *et al.*¹⁵ investigated the active control of flexural wave power flow in 1987. In 1991, Pan and Hansen¹⁶ performed an analysis of the control of power flow. Their study included an investigation into the effect of the orientation of the control actuator. Their results showed, notably, that, in order to control power flow effectively, the control force must be applied within a few degrees of the normal. Pan and Hansen¹⁷ compared the active control of acceleration with the active control of vibration intensity for a beam and found that effective control could be achieved using a single accelerometer error sensor, if the accelerometer was positioned more than about 0.75λ from any sources or discontinuities, where λ represents the structural wavelength. In addition, Elliott and Billet¹⁸ also investigated the control of flexural propagating waves in a beam using a single error accelerometer located in the structural far field. While they did not control the intensity explicitly, they did demonstrate the ability to attenuate the propagation of a broadband excitation in the dispersive medium over a fairly large bandwidth, by minimizing the acceleration at the single far-field sensor.

This paper develops an active control method designed to minimize the structural intensity associated with bending waves in a structure. The method is applicable to applications where the vibration that propagates in a structure is to be minimized. Another possible application involves controlling radiation from structures where the source is coupled to

^{a)}Current address: 1238F East Broad St., Montoursville, PA 17754.

the radiating structure by a defined structural path. In such a case, controlling the structural intensity through this path will also minimize the resulting radiation.

I. CALCULATION OF INTENSITY

A. Description of intensity

The instantaneous structural intensity associated with bending waves in a beam is given at any point as the sum of two terms, which will be referred to as the force term and the moment term. The force term is given by the product of the shear force and transverse velocity and can be expressed as

$$F\nu = EI \frac{\partial^3 \xi}{\partial x^3} \frac{\partial \xi}{\partial t}, \quad (1)$$

where F is the shear force, ν is the transverse velocity, E is Young's modulus, I is the area moment of inertia, and $\xi(x, t)$ is the transverse displacement of the beam. The moment term is given by the product of the bending moment and rotational velocity, and can be expressed as

$$M\Omega = -EI \frac{\partial^2 \xi}{\partial x^2} \frac{\partial^2 \xi}{\partial x \partial t}, \quad (2)$$

where M is the moment and Ω is the rotational velocity. Thus the total instantaneous intensity can be expressed as

$$\Pi = EI \frac{\partial^3 \xi}{\partial x^3} \frac{\partial \xi}{\partial t} - EI \frac{\partial^2 \xi}{\partial x^2} \frac{\partial^2 \xi}{\partial t \partial x}. \quad (3)$$

To gain a greater understanding of some of the control issues, it will be useful to investigate briefly the time-averaged intensity. To this end, consider the problem of controlling the energy propagating in an infinite beam, with an excitation force, $F_n e^{j\omega t}$, located at $x=0$, and a complex control force,

$$\tilde{F}_c e^{j\omega t} = (F_{c,R} + jF_{c,I}) e^{j\omega t}, \quad (4)$$

located at $x=L$, where $j = \sqrt{-1}$. Here, F_n is taken to be real with no loss in generality, and the region of interest is taken to be $x \geq L$. The time-averaged intensity corresponds to the propagating component of the structural intensity and can be expressed as

$$\langle \Pi \rangle_t = \frac{1}{2} \operatorname{Re} \left[EI \frac{\partial^3 \xi}{\partial x^3} \left(\frac{\partial \xi}{\partial t} \right)^* \right] - \frac{1}{2} \operatorname{Re} \left[EI \frac{\partial^2 \xi}{\partial x^2} \left(\frac{\partial^2 \xi}{\partial t \partial x} \right)^* \right]. \quad (5)$$

The two control methods considered are the control of time-averaged intensity and the control of the transverse acceleration at a point $x_0 \geq L$.

The control of time-averaged intensity is considered first. The displacement of the beam can be represented by

$$\xi(x, t) = (j/4EI k^3) (-F_n e^{-jkx} + jF_n e^{-kx} - \tilde{F}_c e^{-jk(L-x)} + j\tilde{F}_c e^{-k(L-x)}) e^{j\omega t}, \quad 0 \leq x \leq L, \quad (6)$$

$$= (j/4EI k^3) (-F_n e^{-jkx} + jF_n e^{-kx} - \tilde{F}_c e^{-jk(x-L)} + j\tilde{F}_c e^{-k(x-L)}) e^{j\omega t}, \quad x \geq L, \quad (7)$$

where k is the flexural wave number. For simplicity, internal structural losses have been neglected in this formulation.

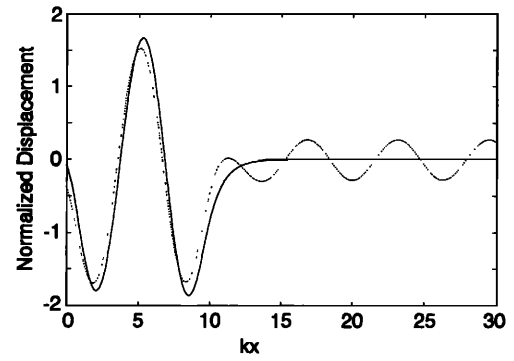


FIG. 1. Beam displacement for the case of minimizing structural intensity (solid line) and acceleration (dotted line). The control source is located at $kL=10$, and the error sensor for minimizing acceleration is located at $kx_0=11$.

Losses can be readily included, but they do not affect the general nature of the results. Performing the necessary derivatives and substituting these expressions into Eq. (5) gives

$$\langle \Pi \rangle_t = \frac{\omega}{32EI k^3} [2F_n^2 + 4F_n F_{c,R} \cos(kL) - 4F_n F_{c,I} \sin(kL) + 2|\tilde{F}_c|^2]. \quad (8)$$

In order to determine the desired control, the time-averaged intensity is minimized with respect to the real and imaginary components of the control force, leading to the optimal control force

$$\tilde{F}_c = -F_n e^{-jkL}. \quad (9)$$

It can be seen that the optimal control force is equal in magnitude to the primary force, with an appropriate phase shift to guarantee force cancellation at the control source location. Substituting this into Eq. (8) leads to $\langle \Pi \rangle_t = 0$ for $x \geq L$, which indicates that no energy propagates past the control source location. Further, substituting Eq. (9) into Eq. (7) yields

$$\xi(x, t) = -(F_n e^{-kx}/4EI k^3) (1 - e^{kL} e^{-jkL}) e^{j\omega t}, \quad x \geq L, \quad (10)$$

indicating that $\xi(x, t)$ decays exponentially to 0 for $x > L$. An example of the displacement field is shown in Fig. 1 for the case where the frequency and source separation are such that $kL=10$. It is important to note that the results obtained for the time-averaged intensity and displacement hold for any location $x_0 \geq L$ of the intensity measurement used for control.

An analogous development can be carried out for the control of the acceleration at a single point, corresponding to an error sensor location. Setting the acceleration at a point, $x_0 > L$, equal to zero and solving for \tilde{F}_c yield

$$\tilde{F}_c = \frac{-e^{-jkx_0} + j e^{-kx_0}}{e^{-jk(x_0-L)} - j e^{-k(x_0-L)}} F_n. \quad (11)$$

Substituting this into the expression for displacement yields an expression that, in general, does not vanish for $x \geq L$. An example of this for the case $kL=10$ is also shown in Fig. 1.

If, however, the point x_0 is far removed from L , such that $k(x_0 - L) \gg 1$, the control force reduces to

$$\tilde{F}_c = -e^{-jkL} F_n. \quad (12)$$

This is the same control force as in Eq. (9) for the case of controlling the time-averaged intensity at any point $x \geq L$. These results are consistent with the work of Pan and Hansen,¹⁷ as well as Elliott and Billet.¹⁸ As is the case with intensity control, substituting this control force into the expression for displacement at $x \geq L$ results in $\xi(x, t)$ decaying exponentially to 0 for $x > L$. Thus controlling acceleration is only effective in general if the error sensor is located far (relative to a wavelength) from the source or any boundaries or discontinuities. In any but the simplest structures, this is difficult if not impossible.

The theoretical advantage of controlling intensity, time-averaged at least, is that the error sensor can be located as close to the control source as geometrical constraints allow. Thus, with complex structures, this suggests that the vibrational energy could be confined to desired regions within the structure.

B. Intensity calculation

A number of ways of determining structural intensity have been studied in the past few years. Sensors ranging from accelerometers, strain gauges, and force gauges to laser velocimeters, vibrometers, and near-field acoustic holography have been employed in this endeavor. In this study, accelerometers are chosen for the measurement of total, instantaneous intensity. A one-dimensional array of five accelerometers positioned on the top of the beam is used. The accelerometer positions are numbered sequentially, with the signal at position i at time t being referred to as $a_{i,t}$.

In Eq. (3) the total, instantaneous intensity is expressed as a function of the transverse displacement. If a time-harmonic vibration with frequency ω_0 is assumed, then the displacement, as a function of the transverse acceleration, can be written as

$$\xi(x, t) = -(1/\omega_0^2) a(x, t). \quad (13)$$

With this expression for ξ , the total, instantaneous intensity at position 3, the center of the array, is expressed as

$$\begin{aligned} \Pi_3 = & EI \left(\frac{-1}{\omega_0^2} \frac{\partial^3 a_3}{\partial x^3} \right) \left(\frac{-1}{\omega_0^2} \frac{\partial a_3}{\partial t} \right) - EI \left(\frac{-1}{\omega_0^2} \frac{\partial^2 a_3}{\partial x^2} \right) \\ & \times \left(\frac{-1}{\omega_0^2} \frac{\partial^2 a_3}{\partial t \partial x} \right) = \frac{EI}{\omega_0^4} \left(\frac{\partial^3 a_3}{\partial x^3} \frac{\partial a_3}{\partial t} - \frac{\partial^2 a_3}{\partial x^2} \frac{\partial^2 a_3}{\partial t \partial x} \right). \end{aligned} \quad (14)$$

In order to evaluate this expression for structural intensity, the various time and space derivatives of the acceleration at position 3 must be estimated.

The time differentials of the accelerations are estimated using a backward finite-difference scheme, with error on the order of τ^2 , where τ is the time increment between samples. A backward finite-difference scheme is used since only those accelerations up to and including the time at which the time derivatives are desired are available. The space differentials

are estimated using a central finite difference scheme, with error on the order of Δ^2 , where Δ is the spacing between accelerometers.

Assuming the necessary partial derivatives have been calculated, the total instantaneous intensity can be estimated. Because the finite-difference operations are performed on accelerations, and not displacements, a double integration must be performed. This double integration is achieved by multiplying each term by $-1/\omega_0^2$, where ω_0 is the frequency of excitation, as shown in Eq. (14). This implies that this method of calculating intensity is only valid for single frequencies, with the frequency of excitation known.

II. CONTROL ARCHITECTURE

This section briefly describes the algorithms used to implement the control systems investigated. Both system identification and control are performed adaptively in real time and will be discussed briefly. The projection algorithm is used for system identification, and the filtered- x least-mean-squares algorithm is used to update the control filters.

A. System Identification

The algorithm used for system identification is the projection algorithm or the normalized least-mean-squares (NLMS) algorithm. In this application of the algorithm, there is assumed to be one error sensor, measuring the error signal, $\epsilon(m)$, where m is a discrete time index. The system identification algorithm estimates the transfer functions correlating the reference input signal and the control signals to this error signal. This method for updating the system identification vectors has been described earlier.⁹ As shown in this earlier work, if $\hat{\Theta}(m+1)$ represents a vector of all the transfer function coefficients used to represent the system, and $\hat{\Phi}(m)$ represents a vector of the control signal outputs and the reference signal inputs, the update equation for the transfer function coefficients can be expressed as

$$\begin{aligned} \hat{\Theta}(m+1) = & \hat{\Theta}(m) + \frac{a\hat{\Phi}(m)}{b + \hat{\Phi}^T(m)\hat{\Phi}(m)} \\ & \times [\epsilon(m) - \hat{\Theta}^T(m)\hat{\Phi}(m)]. \end{aligned} \quad (15)$$

Here, $\epsilon(m)$ is the signal being estimated by the system identification algorithm, a is a convergence parameter (chosen to be $0 < a < 2$ for stability), and b is a small, positive constant used to ensure that there is no division by zero.

B. Control of acceleration

The algorithm used for the control filter update is the filtered- x least-mean-squares algorithm.⁷ This algorithm is used to determine the N control signals, $y_n(m)$, which minimize a mean-squared-error signal. The control signals are obtained by convolving the reference input, $x(m)$, with the control filter coefficients, $W_n(m)$. These control filters are each represented by a finite impulse response (FIR) filter vector with I coefficients:

$$W_n^T(m) \equiv [w_{n0}(m) w_{n1}(m) \cdots w_{n(I-1)}(m)]. \quad (16)$$

The input signal, $x(m)$, is represented in vector form as

$$X^T(m) \equiv [x(m)x(m-1) \cdots x(m-I+1)]. \quad (17)$$

A convolution sum of these two signals gives the n th control output

$$y_n(m) = \sum_{i=0}^{I-1} w_{ni}(m)x(m-i) = W_n^T X, \quad (18)$$

where $w_{ni}(m)$ are the n th control filter coefficients at time m , $y_n(m)$ is the n th control filter output at time m , and $x(m-i)$ is the input to the control filters at time $m-i$. A composite control filter vector can be formed as the concatenation of the N control filter vectors:

$$\mathbf{W}^T(m) \equiv [W_1^T(m) \quad W_2^T(m) \quad \cdots \quad W_N^T(m)]. \quad (19)$$

The optimal solution for the control filter vector is taken to be the solution that minimizes the mean-squared-error signal. The *filtered- x algorithm* is a steepest descent algorithm based on the concept of updating the control filter coefficients according to the negative of the gradient with respect to the filter coefficients of the mean-squared error, so that the control filters converge to the optimal solution in an iterative manner. The mean-squared error is approximated by the instantaneous squared error, $e^2(m)$. This error signal $e(m)$ is not necessarily the same as the error signal used in the system identification algorithm, $\epsilon(m)$. The update equation is expressed as

$$\mathbf{W}(m+1) = \mathbf{W}(m) - \mu_0 \nabla_{\mathbf{w}} e^2(m). \quad (20)$$

The convergence parameter μ_0 is a parameter chosen to ensure convergence and stability, and a method for determining μ_0 has been discussed in earlier literature.¹⁰ The squared error $e^2(m)$, in least-mean-squares-based algorithms, is desired to be quadratic in \mathbf{W} .⁷ Thus, for controlling acceleration, $e(m)$ is equal to the acceleration. This acceleration is chosen to be that at the position 3— a_3 . In this study, one control actuator is used to control the acceleration. There is, therefore, a single control filter and a single control path transfer function filter. Analogous developments have been performed previously,⁹⁻¹¹ and the reader is referred to this literature for a complete development. The result of these developments is that the update equation for the control filter coefficients can be expressed as

$$\mathbf{W}(m+1) = \mathbf{W}(m) - \mu e(m) \mathbf{R}(m), \quad (21)$$

where $\mu = 2\mu_0$ is a parameter chosen to ensure convergence and stability, and $\mathbf{R}(m)$ is the filtered- x reference signal, obtained by convolving the input reference signal with the control path transfer function. One should note that the error signal used for system identification, $\epsilon(m)$, is also the acceleration; that is,

$$\epsilon(m) = e(m) = a_3(m). \quad (22)$$

The two error signals are the same in this case because the filtered quantity that the system identification algorithm is trying to model, \mathbf{R} , corresponds to the same acceleration that the control algorithm is trying to minimize.

C. Control of intensity

The intensity control application of the filtered- x algorithm is not as straightforward as the acceleration control. This is because the total, instantaneous intensity is already a quadratic quantity in \mathbf{W} , unlike the acceleration. This can be seen in that F , ν , M , and Ω are each linear in \mathbf{W} . Therefore, the force term $F\nu$, the moment term $M\Omega$, and, subsequently, the intensity are each quadratic in \mathbf{W} . In order to have $e^2(m)$ quadratic in \mathbf{W} , $e(m)$ is set equal to the square root of intensity. If Π represents the instantaneous intensity, then the update equation can be expressed as

$$\mathbf{W}(m+1) = \mathbf{W}(m) - \mu_0 \nabla_{\mathbf{w}} \Pi. \quad (23)$$

To obtain an expression for the gradient, the intensity can be expressed as

$$\Pi = EI \left(\frac{\partial^3}{\partial x^3} \int \nu dt \cdot \nu \right) - EI \left(\frac{\partial}{\partial x} \int \Omega dt \cdot \Omega \right), \quad (24)$$

where use has been made of the fact that

$$\Omega = \frac{\partial \nu}{\partial x}. \quad (25)$$

Further, if ν and Ω are separated into a primary component (the response with no control) and a component due to the control, they can be represented by

$$\nu = \nu_0 + \mathbf{H}_\nu^T \mathbf{Y}, \quad \Omega = \Omega_0 + \mathbf{H}_\Omega^T \mathbf{Y}, \quad (26)$$

where \mathbf{H}_ν and \mathbf{H}_Ω represent the control path transfer functions from the control signal to the velocity and angular velocity, respectively, at the error sensor array. By interchanging the order of summation, as is done in analogous developments,⁹⁻¹¹ ν and Ω can also be expressed as

$$\nu = \nu_0 + \mathbf{W}^T \mathbf{R}_\nu, \quad \Omega = \Omega_0 + \mathbf{W}^T \mathbf{R}_\Omega, \quad (27)$$

where \mathbf{R}_ν and \mathbf{R}_Ω are given by $\mathbf{H}_\nu^T \mathbf{X}$ and $\mathbf{H}_\Omega^T \mathbf{X}$. Substituting these expressions into Eq. (24), the intensity can be expressed as

$$\begin{aligned} \Pi = EI & \left(\frac{\partial^3}{\partial x^3} \int (\nu_0 + \mathbf{W}^T \mathbf{R}_\nu) dt \cdot (\nu_0 + \mathbf{W}^T \mathbf{R}_\nu) \right) \\ & - EI \left(\frac{\partial}{\partial x} \int (\Omega_0 + \mathbf{W}^T \mathbf{R}_\Omega) dt \cdot (\Omega_0 + \mathbf{W}^T \mathbf{R}_\Omega) \right). \end{aligned} \quad (28)$$

Taking the gradient with respect to \mathbf{W} yields

$$\begin{aligned} \nabla_{\mathbf{w}} \Pi = EI & \left(\frac{\partial^3}{\partial x^3} \int \mathbf{R}_\nu dt \cdot (\nu_0 + \mathbf{W}^T \mathbf{R}_\nu) \right) \\ & + EI \left(\frac{\partial^3}{\partial x^3} \int (\nu_0 + \mathbf{W}^T \mathbf{R}_\nu) dt \cdot \mathbf{R}_\nu \right) \\ & - EI \left(\frac{\partial}{\partial x} \int \mathbf{R}_\Omega dt \cdot (\Omega_0 + \mathbf{W}^T \mathbf{R}_\Omega) \right) \\ & - EI \left(\frac{\partial}{\partial x} \int (\Omega_0 + \mathbf{W}^T \mathbf{R}_\Omega) dt \cdot \mathbf{R}_\Omega \right). \end{aligned} \quad (29)$$

This equation can be simplified by using the expressions for the force and moment. Thus the gradient can be written as

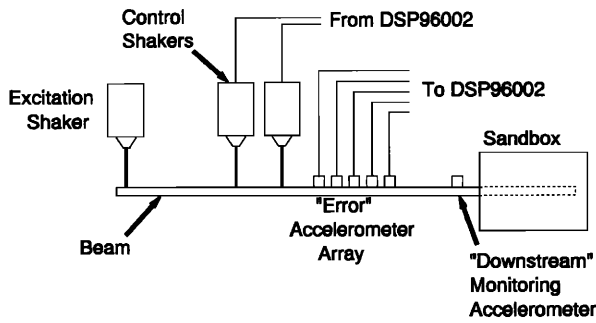


FIG. 2. Schematic of the experimental setup.

$$\nabla_w \Pi = EI \frac{\partial^3}{\partial x^3} \int \mathbf{R}_\nu dt \cdot \nu + F \cdot \mathbf{R}_\nu - EI \frac{\partial}{\partial x} \int \mathbf{R}_\Omega dt \cdot \Omega + M \cdot \mathbf{R}_\Omega. \quad (30)$$

This expression is exact, but it is impractical for implementation on a real-time DSP board. To achieve a practical control scheme for implementation, two sets of heuristic assumptions are used to obtain approximations of this gradient. For the first approximation, the assumptions are made that the third partial derivative with respect to x yields a factor of jk^3 , that the first partial derivative with respect to x yields a factor of $-jk$, and that the integral with respect to time yields a factor of $1/j\omega_0$. (j is again $\sqrt{-1}$, k is the flexural wave number, and ω_0 is the driving frequency.) It should be noted that these assumptions correspond to assuming time-harmonic excitation, and thus implementing the resulting algorithm requires a knowledge of the driving frequency. Using these assumptions in Eq. (30) allows the gradient to be approximated by

$$\nabla_w \Pi \approx \frac{EIk^3}{\omega_0} \mathbf{R}_\nu \cdot \nu + F \cdot \mathbf{R}_\nu + \frac{EIk}{\omega_0} \Omega \cdot \mathbf{R}_\Omega + M \cdot \mathbf{R}_\Omega. \quad (31)$$

One of the possible limitations is that the signs of the various terms depend on the type of wave that is considered. The signs chosen here correspond to a propagating wave in the $+x$ direction. Obviously, if another type of wave dominates the vibration field, some of the phases in the gradient will be wrong, which may affect the performance of the control system. Since \mathbf{R}_Ω and \mathbf{R}_ν correspond to an angular velocity and a transverse velocity, respectively, they are related according to

$$\mathbf{R}_\Omega = \frac{\partial}{\partial x} \{\mathbf{R}_\nu\}. \quad (32)$$

If the derivative is again replaced by $-jk$, \mathbf{R}_Ω can be approximated as

$$\mathbf{R}_\Omega \approx -jk\mathbf{R}_\nu. \quad (33)$$

These results allow the gradient to be approximated as

$$\nabla_w \Pi \approx \mathbf{R}_\nu \left(\frac{EIk^3}{\omega_0} \cdot \nu + F - j \frac{EIk^2}{\omega_0} \cdot \Omega - jkM \right). \quad (34)$$

A simplification of Eq. (34) can be obtained by again assuming a time-harmonic, propagating wave in the $+x$ direction. In this case,

$$F = EI \frac{\partial^3 \xi}{\partial x^3} = \frac{EIk^3}{\omega_0} \nu, \quad M = -EI \frac{\partial^2 \xi}{\partial x^2} = \frac{EIk}{\omega_0} \Omega. \quad (35)$$

Using these results in Eq. (34) allows the gradient to be approximated by

$$\nabla_w \Pi \approx \frac{2EIk^2}{\omega_0} \mathbf{R}_\nu (k\nu - j\Omega). \quad (36)$$

This expression cannot be implemented using the real values obtained from accelerometers. However, the phase shift of $-j$ associated with the angular velocity can be recognized as a time delay in the time domain. If the excitation signal is time-harmonic, as assumed, this phase shift between the two terms in the gradient can be accounted for in the frequency response of the adaptive control filter, which makes it feasible to use a gradient approximation of the form

$$\nabla_w \Pi \approx \frac{2EIk^2}{\omega_0} \mathbf{R}_\nu (k\nu + \Omega). \quad (37)$$

Thus, under the assumptions of a time-harmonic excitation dominated by a propagating wave in the $+x$ direction, the update expression can be expressed as

$$\mathbf{W}(m+1) = \mathbf{W}(m) - \mu e(m) \mathbf{R}_\nu, \quad (38)$$

where

$$e(m) = k\nu + \Omega \quad (39)$$

is the effective error signal for the control algorithm. It should be noted that this is not the effective error signal for the system identification algorithm. The system identification error signal is the velocity, i.e.,

$$e(m) = \nu, \quad (40)$$

since the system identification algorithm is trying to model the filtered quantity \mathbf{R}_ν .

In addition to several possible error signals, three different actuator configurations are considered. These consist of controlling the beam with a control force, a control moment, or both a collocated force and moment. The force output is calculated with one control filter and is sent to two control shakers, such that $y_{c1}(m) = y_{c2}(m) = y_1(m)$, where $y_{ci}(m)$ is the signal to the i th control shaker and $y_1(m)$ is the control filter output. The control shakers are positioned close to each other (relative to a wavelength), so that the effect on the beam approximates a force applied at a point halfway between the shakers.

The moment output is also calculated with one control filter. This moment output is sent phase-reversed to the control shakers, such that $y_{c1}(m) = -y_{c2}(m) = y_2(m)$. For control shakers positioned close to each other, the effect on the beam approximates a moment, or couple, applied at a point halfway between the shakers.

The force-moment actuator configuration for control is a superposition of the force configuration and the moment configuration. The force output is calculated with one control filter, and the moment output is calculated with a second

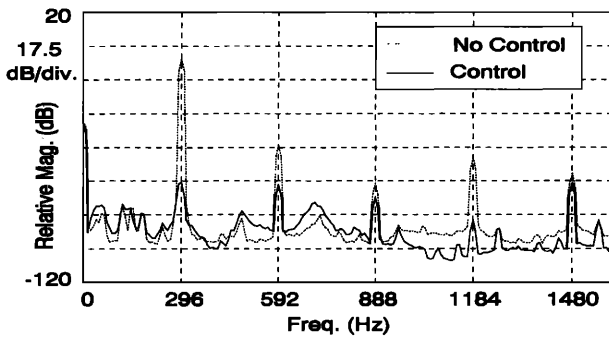


FIG. 3. Error sensor acceleration level with and without control, with the sensor relatively far from the control actuator (296 Hz).

control filter. The force output is sent in phase to both shakers, while the moment output is sent phase-reversed to the two shakers, such that y_{c1} and y_{c2} are given by

$$y_{c1}(m) = y_1(m) + y_2(m), \quad y_{c2}(m) = y_1(m) - y_2(m). \quad (41)$$

III. EXPERIMENTAL SETUP

The system description is divided into two parts: the structure being controlled and the control system implemented to control it. The structure to be controlled in this study consists of a thin-walled, square, hollow steel beam, one end of which is embedded in a box of sand. The other end is supported with a compliant rubber band, in a manner that does not significantly alter the dynamic loading on the beam.

The steel beam has cross-sectional dimensions of 1.6 cm \times 1.6 cm, wall thickness of 1.27 mm, and total length 1.53 m. In addition, the density (ρ) = 7.70×10^3 kg/m³, the cross-sectional area (A) = 74.0×10^{-6} m², the modulus of elasticity (E) = 187×10^9 Pa, and the area moment of inertia (I) = 2.71×10^{-9} m⁴.

One end of the beam is embedded in a box of sand in order to introduce absorption at the boundary and, hence, reduce the magnitude of the reflection coefficient from the value of 1.0 associated with a purely free termination. The length of the beam outside the sand is 1.25 m. A lossless beam and a reflection coefficient of 1.0 at the boundary results in a standing wave field only and, therefore, only reactive (or imaginary) intensity is generated. Reducing the re-

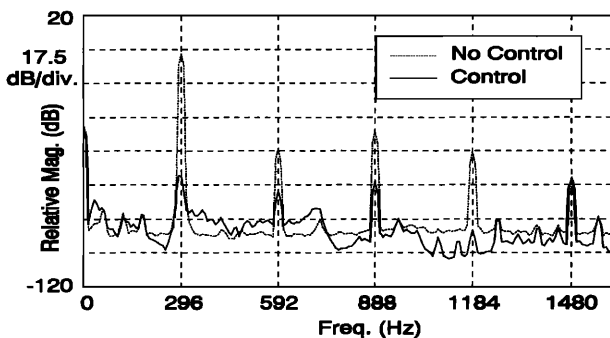


FIG. 4. Error sensor acceleration level with and without control, with the sensor relatively near to the control actuator (296 Hz).

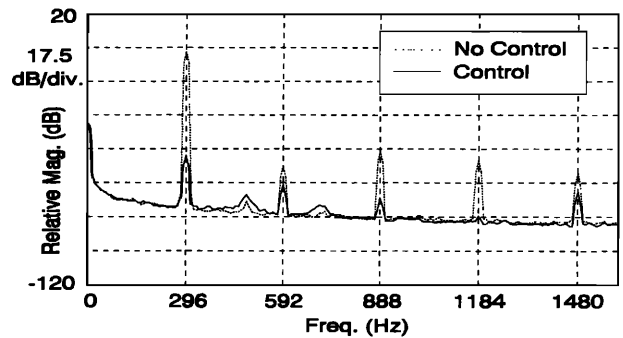


FIG. 5. Far-field acceleration level with and without control, with the sensor relatively far from the control actuator (296 Hz).

flexion coefficient at the boundary reduces the reflected wave and allows the propagating wave component to dominate the wave field. This results in a significant active (or real) intensity component. If the termination is anechoic, corresponding to the reflection coefficient having a value of 0.0, then the intensity is entirely active. Previous studies on beams with the same properties and similar terminations have shown that the reflection coefficient is approximately $0.254 + j0.044$ at 5000 Hz and $0.536 + j0.058$ at 500 Hz.^{14,19} Therefore, for the frequency range used for this study (140–520 Hz), a combination of active and reactive intensity is expected.

The beam is excited at its free end with a Ling Dynamic Systems (LDS) model V203 magnetic driven vibrator. The LDS V203 shaker is connected to the beam by a stinger to insure the delivery of a moment-free transverse force to the beam. The stinger is relatively flexible in its transverse direction, in order to minimize the transfer of any moment to the beam due to misalignment.

The control system consists of three parts: the input sensors, the processor, and the output actuators. The six input signals to the control system originate from five PCB model 336A accelerometers and the signal from the signal generator that drives the primary excitation shaker. The signals from the accelerometers, which have a spacing of 4 cm, are used to calculate the error signals (the error signal in acceleration control is the third acceleration signal). The signal from the signal generator is used as the control filter input $x(m)$. The digital control algorithm is implemented on a Spectrum Signal Processing Inc. DSP96002 digital signal processing

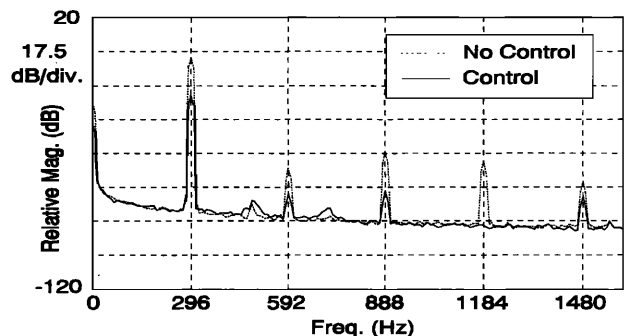


FIG. 6. Far-field acceleration level with and without control, with the sensor relatively near to the control actuator (296 Hz).

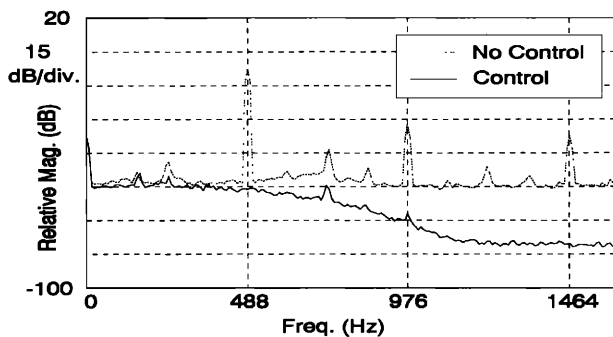


FIG. 7. Typical error function for controlling intensity, with and without control (488 Hz).

board, interfaced with a Spectrum 32-channel 12-bit analog input board and a 16-channel analog output board. For the case of acceleration control there is one output signal, while for the case of intensity control (force only, moment only, or force and moment) there are two output signals. The control shakers used are LDS model V102 magnetic driven vibrators, which also use stingers to control the beam in the same manner as the V203 excitation shaker. A schematic of the experimental setup as described can be seen in Fig. 2.

IV. RESULTS

This section presents some of the experimental results that were obtained using various active control configurations. There are two items that should be noted. The first is that for convenience in examining the following frequency domain plots, the vertical divisions are placed at multiples of the driving frequency. The second is that, because of limits of the output board, the intensity and error function signals are scaled to avoid clipping while realizing the resolution potential of the D/A converter. This scaling of the signals is invariant within a given setup/frequency permutation. The result is that specific values are compared within a setup/frequency permutation; however, only relative reductions are to be compared otherwise.

There are several aspects of the control results examined. First, we discuss the method of controlling acceleration, which works significantly better with the error sensor positioned relatively far from, rather than relatively near to, the control actuator. It is desired to have the sensors in either

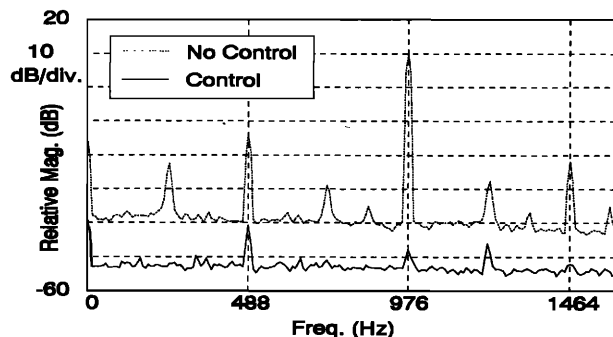


FIG. 8. Intensity estimated from the error sensor array, with and without control (488 Hz).

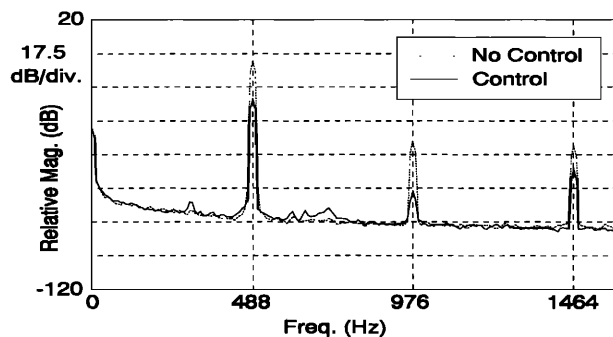


FIG. 9. Far-field acceleration level with and without control when controlling the intensity with the sensor array relatively far from the control source (488 Hz).

the near field or the far field. However, because of the length of the beam, there are some cases where it is not possible to have the sensors far enough away from the control source to say conclusively that the sensors are in the far field. Thus the terminology “relatively near” and “relatively far” has been adopted to distinguish the two error sensor configurations. The case of relatively near corresponds to a spacing between the control shakers and the sensor array (center to center) of 15 cm, while relatively far corresponds to a spacing of 75 cm. Second, we discuss the general trends of controlling structural intensity with the error sensor positioned relatively far from the control actuator. A third aspect examined is intensity control with the error sensor positioned relatively near to the control actuator. Related to this is a discussion of the general trend of frequency dependence associated with controlling intensity. Finally, a brief discussion is given of the trends in actuator configuration dependence for intensity control.

It was shown earlier that controlling the acceleration of the beam should be much more effective with the error sensor positioned relatively far from, rather than relatively near to, the control actuator. Figures 3 and 4, for forced excitation at 296 Hz, show the local acceleration at the error accelerometers when the acceleration is controlled with the error sensor located relatively far from or near to the control actuator, respectively. For both configurations, the local attenuation is comparable, with the error acceleration being attenuated by over 60 dB in both cases. However, if one examines

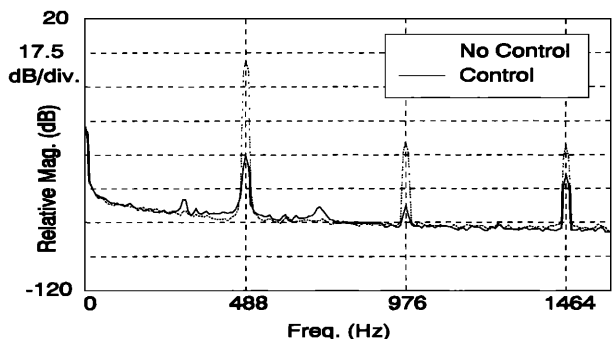


FIG. 10. Far-field acceleration level with and without control when controlling the acceleration with the error sensor relatively far from the control source (488 Hz).

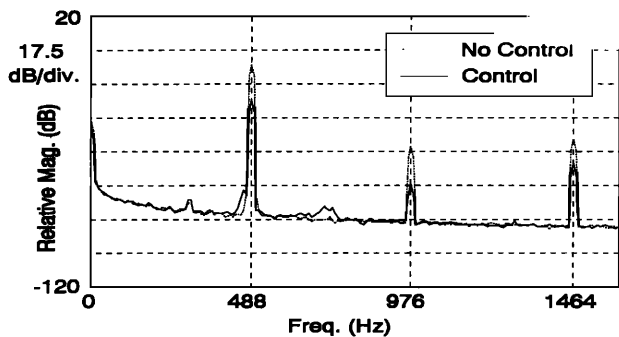


FIG. 11. Far-field acceleration level with and without control when controlling the intensity with the sensor array relatively near to the control source (488 Hz).

Figs. 5 and 6, this comparable reduction in the error acceleration does not result in comparable reductions in the downstream acceleration signal. In Fig. 5, it can be seen that controlling acceleration with the error sensor positioned relatively far from the control actuator results in more than a 50-dB reduction in the downstream acceleration signal, while in Fig. 6 it can be seen that controlling acceleration with the error sensor positioned relatively near to the control actuator results in approximately a 20-dB reduction in the downstream acceleration signal. These results are in agreement with the expectations discussed above.

It was noted earlier that controlling the intensity and controlling the acceleration should yield comparable results with the error sensor located in the farfield. Figure 7, for forced excitation at 488 Hz, shows a representative example of the error function signal when controlling intensity for the error sensor in either the near field or the far field. One can see that the error function signal is attenuated by approximately 50 dB. The intensity signal, as shown in Fig. 8, also at 488 Hz, is reduced as well. The peak at $2\omega_0$, 976 Hz, is reduced on the order of 55 dB, while the dc value is reduced approximately 22 dB. The downstream acceleration signal for an excitation frequency of 488 Hz is reduced approximately 20 dB (Fig. 9) through implementation of this intensity control scheme. This is in contrast to the more than 40-dB reduction in the downstream acceleration achieved through the implementation of the acceleration control scheme, as shown in Fig. 10. The fact that the acceleration

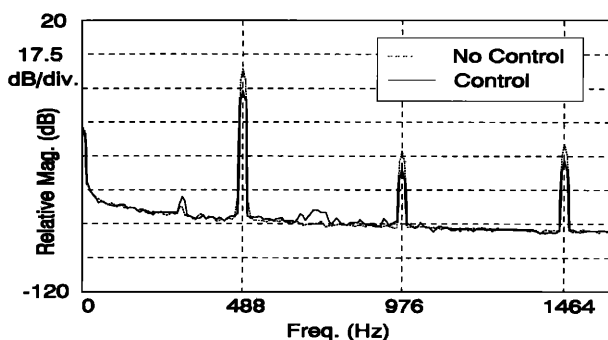


FIG. 12. Far-field acceleration level with and without control when controlling the acceleration with the error sensor relatively near to the control source (488 Hz).

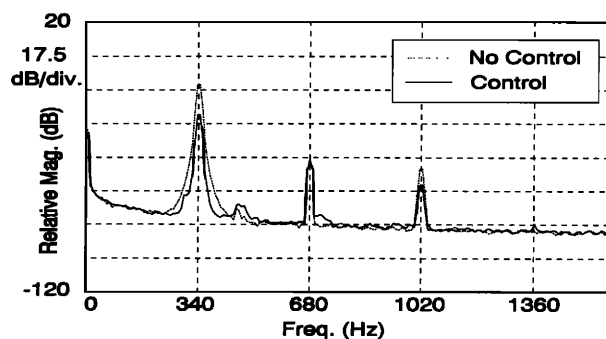


FIG. 13. Far-field acceleration level with and without control when controlling the intensity with the sensor array relatively near to the control source (340 Hz).

control performs better than the intensity control when the error sensor is positioned relatively far from the control actuators is not surprising, because of the numerical noise associated with the finite-difference schemes degrading the error function signal.

With the error sensor positioned relatively near to the control actuators, the theory presented above indicates that the intensity control should outperform the acceleration control. The results obtained over the range of configurations tested are not conclusive, but seem to indicate that it is possible to obtain improved attenuation using intensity control. Figure 11 shows the control achieved for a 488-Hz excitation when the intensity was controlled with the error sensor near the control actuators, while Fig. 12 shows the corresponding control achieved when the acceleration was controlled. The reduction in the downstream acceleration is on the order of 17 dB when controlling the intensity, while the reduction when controlling the acceleration is approximately 10 dB. Another example of intensity control performing better than acceleration control is shown in Figs. 13 and 14. In Fig. 13, the downstream acceleration signal resulting from intensity control at 340 Hz is shown to be attenuated by approximately 17 dB. This is compared to the reduction in downstream acceleration resulting from acceleration control, which is shown in Fig. 14 to be approximately 4 dB. However, it should be noted that in a number of the tests run, the intensity control does not perform as well as the acceleration control. In performing the tests, several trends are identified

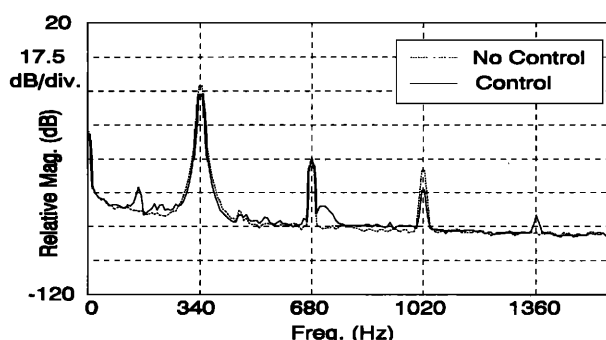


FIG. 14. Far-field acceleration level with and without control when controlling the acceleration with the error sensor relatively near to the control source (340 Hz).

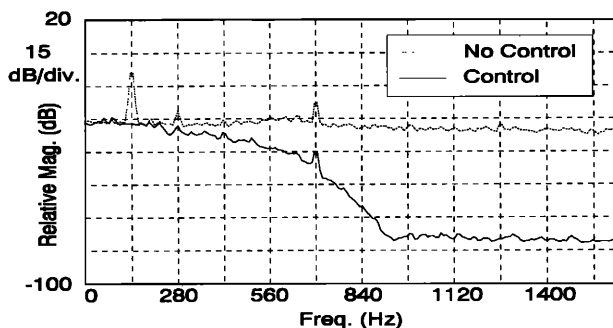


FIG. 15. Error function for controlling intensity with the error sensor array relatively near to the control source (140 Hz).

that may contribute to these difficulties. Some of these trends and problems will be identified below.

One problem associated with intensity control is that of frequency dependence, in that the control scheme tends to work better at higher frequencies. It is thought that this occurs because the error function has a higher signal-to-noise ratio (SNR) at these higher frequencies. Figures 15 and 16 show two representative examples. The error signal in Fig. 15 (140 Hz) has a SNR of about 25 dB, while the SNR in Fig. 16 (488 Hz) is about 45 dB. For the corresponding attenuation of the downstream acceleration, the acceleration is essentially unchanged at 140 Hz, while an attenuation of about 17 dB is observed at 488 Hz. One possible contribution to this frequency dependence involves the accelerometer spacing in terms of the flexural wavelength λ . The spacing between accelerometers is 4 cm. At the highest frequency tested (520 Hz), this corresponds to about 0.067λ , while at the lowest frequency (140 Hz), this accelerometer spacing corresponds to about 0.034λ . For the spatial finite differencing schemes used, neighboring acceleration values are subtracted in order to approximate the spatial derivatives. If these signals are almost equal, more error will be introduced with a finite bit accuracy processor than if the signals are not almost equal. Lower frequencies correspond to positioning the accelerometers closer, relative to a wavelength, which ensures that the neighboring values will be almost equal.

An additional contribution to the frequency dependence involves the ratio of the driving frequency to the sampling frequency. This effect is analogous to the one for geometrical spacing just discussed. Successive (in time) signals are sub-

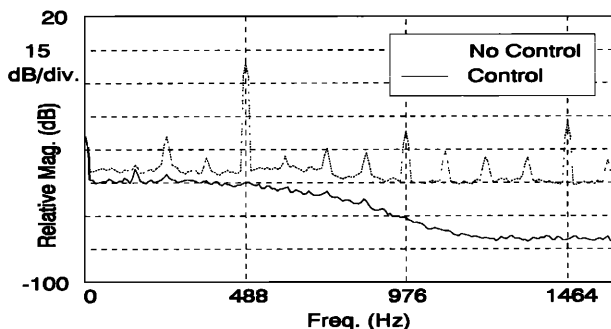


FIG. 16. Error function for controlling intensity with the error sensor array relatively near to the control source (488 Hz).

tracted to give an approximation of the time derivatives. The closer these signals are to being equal, the more processing error will be introduced into the derivative approximation. Thus sampling the lower-frequency signals at a relatively high sampling frequency ensures that the successive samples are closer to being equal in value and leads to larger errors. The sampling frequency here was chosen to be 8 kHz, which works quite well for the higher frequencies, but not as well for the lower frequencies (<300 Hz).

A final contribution to the frequency dependence concerns the structural wavelength relative to the error sensor location and beam length. One should recall that a $+x$ traveling wave is assumed in the development of the intensity error functions. At lower frequencies, the wavelength increases, which increases the range over which evanescent waves are significant. The more the field is affected by waves other than $+x$ traveling waves, the less valid the error function is, and the less the calculated error function relates to the true gradient of intensity.

A final issue concerning intensity control is that of control actuator configuration dependence. For the configurations tested, it was found that there are no strong performance trends in using a force actuator, a moment actuator, or both. The control obtained using any of these configurations was found to be comparable.

V. CONCLUSIONS

The goals of this study were to develop, implement, and evaluate several algorithms for the adaptive vibration control of the total, instantaneous structural intensity in a beam. A measurement algorithm based on finite-difference schemes was developed for calculating the necessary partial derivatives in both space and time. A control algorithm based on the filtered- x algorithm was developed to minimize the structural intensity in the beam. The various intensity control schemes were evaluated relative to acceleration control by means of a downstream acceleration signal. Evaluation of the results from these tests lead to several conclusions.

The first conclusion is that acceleration control was more effective with the error sensor in the far field than in the near field, which was predicted. Furthermore, with the error sensors positioned relatively far from the control actuators, controlling acceleration was more effective than controlling intensity, using the algorithms developed in this study. Although theory predicts that the two schemes should perform equally well, noise in the effective error signal degrades the effectiveness of the intensity control algorithm.

With the error sensors positioned relatively near to the control actuators, the attenuation achieved by controlling intensity was comparable to or greater than that achieved by controlling acceleration. It was predicted that this attenuation should always be greater when controlling intensity than when controlling acceleration. It is thought that the reasons for the degraded performance when controlling the intensity include the frequency dependence of the control schemes and numerical noise in the computation of the error function signal. Signal noise was a problem at all frequencies. This noise consists of electronic noise from the accelerometers and numerical noise from the finite-difference techniques.

Based on the results obtained, it is felt that the effectiveness of the method of controlling structural intensity is limited by the accuracy of the intensity estimate. As better methods of determining the structural intensity are developed, it is anticipated that the effectiveness of the method will increase correspondingly.

- ¹H. F. Olson, "Electronic control of noise, vibration, and reverberation," *J. Acoust. Soc. Am.* **28**, 966–972 (1956).
- ²J. A. Bonesho and J. G. Bollinger, "How to design a self-optimizing vibration damper," *Machine Design* **40**, 123–127 (1968).
- ³C. E. Kaplow and J. R. Velman, "Active local vibration isolation applied to a flexible space telescope," *J. Guidance Control* **3**, 227–233 (1980).
- ⁴T. Bailey and J. E. Hubbard Jr., "Distributed piezoelectric-polymer active vibration control of a cantilever beam," *J. Guidance Control* **8**, 605–611 (1985).
- ⁵C. R. Johnson, Jr., "Adaptive modal control of large flexible spacecraft," *J. Guidance Control* **3**, 369–375 (1980).
- ⁶H. Öz and L. Meirovitch, "Optimal modal-space control of flexible gyroscopic systems," *J. Guidance Control* **3**, 218–226 (1980).
- ⁷B. Widrow and S. D. Stearns, *Adaptive Signal Processing* (Prentice-Hall, Englewood Cliffs, NJ, 1985).
- ⁸S. J. Elliott, I. M. Stothers, and P. A. Nelson, "A multiple error LMS algorithm and its application to the active control of sound and vibration," *IEEE Trans. Acoust. Speech Signal Process.* **ASSP-35**, 1423–1434 (1987).
- ⁹S. D. Sommerfeldt and J. Tichy, "Adaptive control of a two-stage vibration isolation mount," *J. Acoust. Soc. Am.* **88**, 938–944 (1990).
- ¹⁰S. D. Sommerfeldt, "Multi-channel adaptive control of structural vibration," *Noise Control Eng. J.* **37**, 77–89 (1991).
- ¹¹S. D. Sommerfeldt and P. J. Nashif, "Energy based control of the sound field in enclosures," in *Proceedings of the Second International Congress on Recent Developments in Air- & Structure-Borne Sound and Vibration* (Mechanical Engineering Dept., Auburn University, Auburn, AL 1992), Vol. 1, pp. 361–368.
- ¹²D. U. Noiseux, "Measurement of power flow in uniform beams and plates," *J. Acoust. Soc. Am.* **47**, 238–247 (1970).
- ¹³G. Pavic, "Measurement of structure borne wave intensity, Part I: Formulation of the methods," *J. Sound Vib.* **49**, 221–230 (1976).
- ¹⁴S. I. Hayek, M. J. Pechersky, and B. T. Suen, "Analysis and measurement of near- and far-field structural intensity by laser vibrometry," in *Proceedings of the Third International Conference on Structural Intensity* (Centre Technique des Industries Mecaniques, Senlis, France, 1990), pp. 281–288.
- ¹⁵W. Redman-White, P. A. Nelson, and A. R. D. Curtis, "Experiments on the active control of flexural wave power flow," *J. Sound Vib.* **112**, 187–191 (1987).
- ¹⁶J. Pan and C. H. Hansen, "Active control of total vibratory power flow in a beam. I: Physical system analysis," *J. Acoust. Soc. Am.* **89**, 200–209 (1991).
- ¹⁷X. Pan and C. H. Hansen, "The effect of error sensor location and type on the active control of beam vibration," *J. Sound Vib.* **165**, 497–510 (1993).
- ¹⁸S. J. Elliott and L. Billet, "Adaptive-control of flexural waves propagating in a beam," *J. Sound Vib.* **163**, 295–310 (1993).
- ¹⁹S. H. Tousi, "Complex impedances of structural terminations" B. S. thesis, The Pennsylvania State University, University Park, PA (1991).